JOURNAL OF GUIDANCE, CONTROL, AND DYNAMICS
Vol. 41, No. 11, November 2018

Elliptic Guidance

Riley Livermore,* Ronny Tsalik,† and Tal Shima‡
Technion–Israel Institute of Technology, Haifa 32000, Israel

DOI: 10.2514/1.G003565

A new three-point guidance concept for imposing a launch angle, impact angle, and intercept time against a stationary target is proposed. The guidance concept is based on the defining geometric rule of an ellipse. This rule states that, for every point along an ellipse, the sum of the distances to the two focal points is constant. A general method for finding the desired elliptical trajectory that achieves a desired launch angle, impact angle, and intercept time is presented. Once the elliptical trajectory is determined, the sum of the distances between the interceptor and the two foci is the only information required for implementation. The interceptor's equations of motion are linearized around the desired elliptical trajectory, and a proportional–integral–derivative controller is used to implement the elliptical geometric rule. Nonlinear simulations are performed for an interceptor imposing different impact angles with the same intercept time as well as different intercept times at the same impact angle, both against a stationary target. The effects of initial heading errors and first-order interceptor dynamics are also examined.

I. Introduction

SHAPING an interceptor's trajectory to achieve a specific intercept time or impact angle has large ramifications on target survivability, warhead size, collateral damage, and possible coordination efforts with other interceptors. A wide variety of guidance laws that enforce a specific impact angle, an intercept time, or both have been documented in the open literature. Some key characteristics distinguishing these approaches are the underlying guidance concepts and how they are implemented.

A classic example of a guidance concept that can be used for intercept time and impact angle guidance is deviated pure pursuit (DPP). DPP is an extension of the pure pursuit geometric rule in that the interceptor maintains a constant bias from the line of sight (LOS) vector. The interceptor's impact angle is only dependent on the LOS bias angle and the speed ratio between the interceptor and the target [1]. In [2], an optimal control-based guidance law was used to implement the DPP geometric rule to enforce either an intercept time or angle against a nonmaneuvering target. The main advantage of using DPP is that it is simple to implement and only requires knowledge of the target's speed and the LOS to work.

The parallel navigation geometric rule serves as the underlying guidance concept for a wide variety of guidance laws. A popular solution strategy is to assume small deviations from a collision triangle and to use optimal control methods or differential game theory [3–5] to develop the guidance law. These guidance laws can be successfully implemented to solve the terminal intercept angle and time problems if the interceptor does not deviate substantially from the collision triangle geometry during the endgame phase of the engagement. The first appearance of an impact-angle guidance law using optimal control was in [6]. The proposed guidance law was developed by solving a linear quadratic control problem of a reentry vehicle intercepting a nonmaneuvering target with a constraint on its impact angle. Similar guidance laws have been developed in [7–9] that solve linear optimal control problems to enforce a specific intercept angle. In these approaches, a performance index involving the interceptor's control, impact angle, and miss distance is minimized.

Linearization around a collision triangle was also used to develop an optimal guidance law that achieved a specific impact time against a stationary target in [10]. The guidance law was developed by formulating the intercept time as a path constraint and minimizing the interceptor's acceleration throughout the engagement. In [11], an extra degree of freedom was added to the system by controlling the jerk instead of the acceleration of the missile. This additional degree of freedom enabled the interceptor to achieve both an intercept time and angle simultaneously. The guidance law in [12] enforced both an impact time and angle using a polynomial guidance law. Polynomial guidance [13] was developed based on small deviations from a collision triangle and expresses the interceptor's time to go (t_{go}) as a polynomial function. Overall, the benefit of linearizing around the collision triangle is that it enables the use of linear controller strategies and oftentimes leads to analytical solutions. However, the accuracy of these guidance laws degrades when there are large deviations from the collision triangle during the endgame phase of the engagement.

Biased proportional navigation (BPN) is another prominent guidance concept that has been used for imposing a terminal intercept angle and time. Using a form of BPN, Lu et al. [14] developed an adaptive framework for determining the proportional navigation gain that guided a hypersonic vehicle toward a stationary target. The guidance laws in [15–19] imposed a specific impact angle by dividing the missile trajectory into two distinct phases. The differences in [15–19] lie in the gain values selected for each phase as well as the switching time between the phases. Additionally, Liu et al. [20] obtained a desired impact angle by continuously solving a closed-loop, optimal-control problem to update the proportional navigation gain. Zhang et al. [21] extended the use of BPN to enforce both an intercept angle and time by incorporating a t_{go} estimate in the gain calculation.

Other guidance concepts developed for imposing intercept times and angles have been implemented using nonlinear guidance laws. A new guidance concept was proposed in [22] that enabled an interceptor to impose a predefined angle relative to the target's velocity vector. The guidance law was developed using the nonlinear, robust sliding-mode control (SMC) methodology [23]. Similarly, Kumar et al. [24,25] defined the terminal impact angle in terms of a desired LOS and used SMC to shape the missile's normal acceleration. In [26], an LOS rate shaping process was developed for an interceptor to achieve both a specific intercept time and angle and was implemented using a second-order SMC.

Geometric guidance concepts featuring circular trajectories have also been used for intercepting targets at a specific angle. In [27], a circular navigation guidance law was developed and implemented using the instantaneous approach angle of the missile relative to the target. Similarly, Yoon [28] developed a guidance law that imposed a

Received 14 January 2018; revision received 26 April 2018; accepted for publication 26 April 2018; published online 29 June 2018.

*Visiting Researcher, Department of Aerospace Engineering; livermore@technion.ac.il.

†Ph.D. Student, Department of Aerospace Engineering; rtsalik@tx.technion.ac.il.

‡Professor, Department of Aerospace Engineering; tal.shima@technion.ac.il. Associate Fellow AIAA.

specific impact angle using a circular reference curve relative to a moving target.

The guidance laws found in [2,6–22,24–29] are considered to be two-point guidance laws. In two-point guidance laws, only the interceptor and the target are considered. This means that the successful implementation of the guidance concept is dependent on the interceptor's ability to measure or estimate all of the required parameters (e.g., LOS, target heading and velocity). Furthermore, in the cases where both an intercept time and impact angle are independently enforced [11,12,21,26], an extra degree of freedom is required in the guidance law. This extra degree of freedom results in greater guidance law complexity because more information is required (e.g., t_{go} and LOS rate).

A three-point guidance concept approach incorporates a third party. Tsalik and Shima [30,31] proposed a new, three-point guidance law called inscribed angle guidance, which can be used to enforce an intercept angle. This guidance concept capitalizes on the unique geometric principle that a constant inscribed angle between the launcher, missile, and target necessitates a circular trajectory. Therefore, only the inscribed angle is required to implement the guidance law. The downside of using circular trajectories is that there is only one degree of freedom, namely, the origin (focus) of the circle. This single degree of freedom means that each nominal trajectory has only one unique launch angle, impact angle, and intercept time. Extending the scope of a geometric guidance concept with a single focus to two foci adds two additional degrees of freedom (distance and angle between the foci) that allow for the launch angle, impact angle, and intercept time to be determined independently.

Hyperbolas and ellipses are the two types of conic sections that have two foci. Hyperbolas are defined by the difference of the distances between the two foci being constant. Hyperbolic guidance strategies [32] capitalize on this principle by picking the desired distance between the two foci to form the missile's trajectory. Unfortunately, no uses of hyperbolic guidance to impose a specific intercept time or angle have been found in the open literature.

There are also a few cases where elliptical trajectories have been used for missile guidance applications. In [33], elliptical trajectories were developed for a missile to intersect a stationary target at a specific angle. Additionally, Reidel et al. [34] used elliptical trajectories to impose a terminal intercept angle for the Tomahawk missile. Depending on the initial conditions of the missile, the Tomahawk would converge to the closest ellipse that intersected the target at the desired impact angle. In both [33,34], the guidance laws that maintained the missile along the elliptical trajectories were not shown.

This paper presents a new three-point guidance concept and a linear guidance law that imposes a launch angle, impact angle, and intercept time against a stationary target. The foundation of this guidance concept is the elliptical geometric rule that states that the sum of the distances between any point along an ellipse and the two foci of that ellipse is constant. This elliptical guidance concept is beneficial because it has three degrees of freedom (the origin of the ellipse, the rotation angle of the ellipse, and the distance between the foci), and a control scheme can be designed around one variable (sum of the distances between the interceptor and the two foci). The three degrees of freedom allow for a range of launch angles to be achieved for a defined impact angle and intercept time, and the single control parameter allows for the development of a simple and implementable guidance law. The result is a flexible framework for achieving a range of intercept times and angles that can be implemented without calculating time-varying variables like t_{go} and LOS rate. The simplicity of implementation distinguishes this elliptic guidance concept from other similar impact angle and intercept time guidance laws [11,12,21,26].

This paper is organized as follows. The equations of motion are formulated in Sec. II. The new guidance concept and implementation strategy is presented in Sec. III. The method for finding the desired elliptical trajectories is developed in Sec. IV. Section V presents the guidance law development. Section VI contains simulations for various scenarios. And Sec. VII concludes on the findings of this research.

II. Equations of Motion

The engagement between the interceptor and the target is formulated as a surface-to-surface, planar interception problem. The interceptor is assumed to travel at a constant speed V from a stationary launcher L clockwise around an elliptical trajectory toward a stationary target T. The problem is formulated using both a Cartesian and polar coordinate frame. The Cartesian frame is used for the simulations of the guidance law, whereas the polar frame is used for deriving the linear guidance law.

A. Cartesian Frame

The problem is initially formulated in the Cartesian frame, and the engagement geometry is displayed in Fig. 1. The equations of motion for an ideal missile in the Cartesian frame are given as

$$\dot{x} = V\cos\gamma \tag{1a}$$

$$\dot{y} = V\sin\gamma \tag{1b}$$

$$\dot{\gamma} = \frac{a_M}{V} \tag{1c}$$

The missile acceleration a_M is measured orthogonal to the velocity vector, and the missile's flight-path angle γ is measured relative to the inertial frame. The angle θ, called the eccentric anomaly in orbital mechanics, is an angular parameter that gives the relative location of the missile along the elliptical trajectory. To correspond with the definition of γ, θ is measured clockwise. The Euclidean distances between the two foci (f_1, f_2) to the missile are marked as d_1 and d_2, respectively.

The major axis of the ellipse is a, and the minor axis is b. The distance from the origin to either focus is $c = \sqrt{a^2 - b^2}$. The angle between L and T is ξ. Finally, the general parametric equations for an ellipse rotated by λ about its origin, $[x_0, y_0]$, in the inertial Cartesian frame are

$$x = -a\cos\theta\cos\lambda + b\sin\theta\sin\lambda + x_0 \tag{2a}$$

$$y = a\cos\theta\sin\lambda + b\sin\theta\cos\lambda + y_0 \tag{2b}$$

B. Polar Frame

Although the Cartesian frame is intuitive and the equations of motion [Eq. (1)] are straightforward, the equations for a nominal elliptical trajectory are better suited to the polar frame. A nominal trajectory is essential to developing and analyzing a linear guidance law for the proposed guidance concept. Therefore, a polar coordinate frame is used for developing the equations of motion of the ellipse to simplify the linearization process. Figure 2 presents the engagement geometry in the polar frame.

The origin of the polar frame is located at f_1, and the radial ($\boldsymbol{e}_{d_1}$) and the rotational ($\boldsymbol{e}_{\psi}$) directions make up the two axes. The rates of change along these two axes are

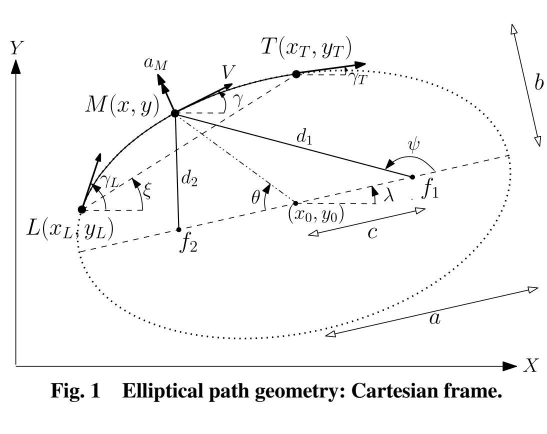

Fig. 1 Elliptical path geometry: Cartesian frame.

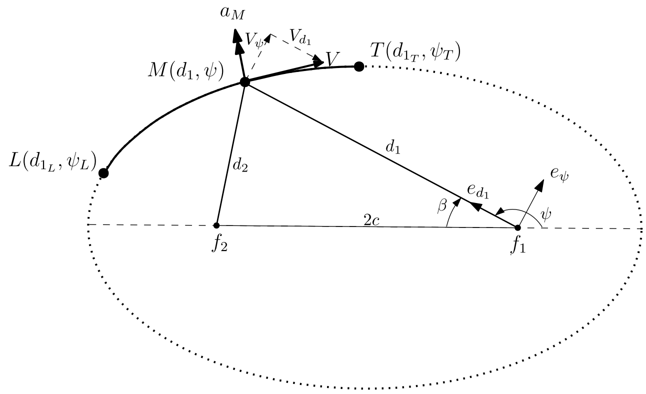

Fig. 2 Elliptical path geometry: polar frame.

$$\dot{d}_1(t) = -V_{d_1}(t) \tag{3a}$$

$$\dot{\psi}(t) = -\frac{V_\psi(t)}{d_1(t)} \tag{3b}$$

Similar to the Cartesian frame, the acceleration of the interceptor is orthogonal to the velocity vector, which is the vector sum of the two velocity components in the polar frame (V_ψ and V_{d_1}). The time rates of change of V_{d_1} and V_ψ are given as

$$\dot{V}_{d_1}(t) = \frac{V_\psi(t)^2}{d_1(t)} - \frac{V_\psi(t) a_M(t)}{V} \tag{4a}$$

$$\dot{V}_\psi(t) = -\frac{V_{d_1}(t) V_\psi(t)}{d_1(t)} + \frac{a_M(t) V_{d_1}(t)}{V} \tag{4b}$$

The elliptic guidance concept is dependent on the sum of the distances from each focus. Therefore, the value of d_2 is found using the law of cosines, yielding

$$d_2 = \sqrt{d_1^2 + 4c^2 - 4 d_1 c \cos\beta} \tag{5}$$

where

$$\beta = \pi - |\psi| \tag{6}$$

The absolute value of ψ is used in Eq. (6) to ensure that β is the supplementary angle of ψ (given $-\pi < \psi < \pi$). Last, the ellipse in the polar frame can be mapped back into the Cartesian frame using the following parametric equations:

$$x = c + d_1 \cos\psi + x_0 \tag{7a}$$

$$y = d_1 \sin\psi + y_0 \tag{7b}$$

III. New Guidance Concept

The new elliptic guidance concept is presented in this section. First, the guiding geometric rule is defined, followed by a recommended implementation strategy for executing the guidance concept.

A. Geometric Rule

The proposed three-point elliptic guidance concept is based on the defining geometric rule of an ellipse, which states the following.

Theorem 1: The sum of the distances between any point along an ellipse and the two focal points of that ellipse are constant and equal to twice the length of the semi-major axis.

Proof: See [35]. □

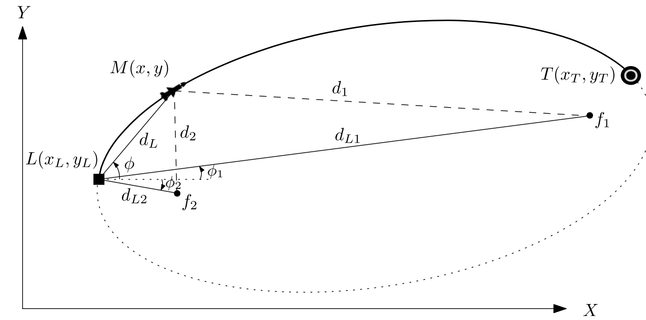

Fig. 3 Implementation of elliptic guidance for launcher–target scenario.

The location of the ellipse's origin, the angle of rotation of the ellipse, and the distance between the origin and the foci provide three degrees of freedom for manipulating the interceptor's trajectory. Smartly picking the location of each focus allows the elliptical trajectory to be customized to intercept the stationary target at a desired intercept time t_f^* and at desired launch and impact angles (γ_L^* and γ_T^*). Once the foci locations are determined, the distances between them and the interceptor can be measured. The sum of these two distances is given as

$$D = d_1 + d_2 \tag{8}$$

This total distance is subtracted from twice the major axis to give the deviation error of the interceptor from the desired elliptical trajectory:

$$e = 2a - D \tag{9}$$

The only parameter required for the successful enforcement of this guidance concept is D. As a result, this elliptical guidance concept gives a simple framework for following along an elliptical trajectory.

B. Implementation

The concept of measuring distances from the interceptor to the foci is simple in theory but can be difficult in implementation. In a real-world scenario, a physical device would be required at each focus to serve as a beacon for the interceptor. Because the foci locations are functions of the desired ellipse, these devices would be required to move potentially large distances, depending on the desired launch angle, impact angle, and intercept time. Therefore, an alternative approach using virtual foci is proposed. Figure 3 shows schematically how the two distances from these virtual foci to the interceptor are measured relative to the launcher's location.

In Fig. 3, the launcher is the reference point for determining the distances and the angles to the two foci (f_1 and f_2) and the interceptor. Because the launcher and two foci are stationary throughout the engagement, d_{L1}, d_{L2}, ϕ_1, and ϕ_2 are constant and can be calculated from the launcher. The distances from the interceptor to the foci are calculated using the law of cosines:

$$d_i = \sqrt{d_L^2 + d_{Li}^2 - 2 d_L d_{Li} \cos(\phi - \phi_i)}, \qquad i \in \{1, 2\} \tag{10}$$

The only time-varying parameters in Eq. (10) are the distance d_L and the angle ϕ of the interceptor to the launcher, and both of them can be measured by the launcher. All the other variables are known a priori and are constant throughout the engagement. Therefore, the error value of the interceptor [Eq. (9)] can be calculated by the launcher and sent via uplink to the interceptor. This process minimizes the hardware required by the missile, while maintaining the integrity of the guidance concept.

IV. Trajectory Design

The proper implementation of the elliptic guidance concept is dependent on knowing the locations of the desired ellipse's foci. This section outlines the process used to find the desired elliptical trajectory. First, the general equations that define an elliptical trajectory for γ_L^*, γ_T^*, and t_f^* are presented. Next, a special case is developed that gives closed-form equations for a subset of ellipses that meet γ_T^* and either γ_L^* or t_f^*. Third, an algorithm outlining a solution strategy for finding the elliptical trajectory that satisfies γ_L^*, γ_T^*, and t_f^* is presented. Last, the algorithm is applied in a case study.

A. General Case

The process for finding an ellipse that satisfies γ_L^*, γ_T^*, and t_f^* can best be understood by first looking at how the foci of that ellipse are defined. The foci f_1 and f_2 are defined in the inertial Cartesian frame as

$$f_{1_x} = x_0 + c\cos\lambda \tag{11a}$$

$$f_{1_y} = y_0 + c\sin\lambda \tag{11b}$$

$$f_{2_x} = x_0 - c\cos\lambda \tag{11c}$$

$$f_{2_y} = y_0 - c\sin\lambda \tag{11d}$$

Four variables define the location of the foci in Eq. (11): the origin of the ellipse (x_0 and y_0), the distance from the origin to each foci (c), and the angle of rotation of the ellipse (λ). The values of x_0 and y_0 are coupled because the elliptical trajectory must intersect both L and T. This leaves three degrees of freedom, which means that three equations are required.

Two of the three equations come from the flight-path angle γ of the interceptor, which is defined in the inertial Cartesian frame as

$$\tan(2\gamma) = -\frac{(y - f_{1_y})(x - f_{2_x}) + (y - f_{2_y})(x - f_{1_x})}{(y - f_{1_y})(y - f_{2_y}) - (x - f_{1_x})(x - f_{2_x})} \tag{12}$$

The first equation accounts for the flight-path angle of the interceptor at L ($\gamma = \gamma_L^*$, $x = x_L$, and $y = y_L$), and the second equation accounts for the interceptor's flight-path angle at T ($\gamma = \gamma_T^*$, $x = x_T$, and $y = y_T$). Because of the constant-speed assumption, the arc length of the ellipse is directly correlated with t_f^*. The equation for the arc length of an ellipse yields the third equation needed in the formulation. The equation that gives the arc length of an ellipse is known as the elliptical integral of the second kind and is defined as

$$\mathbb{L} = a\int_{\theta_L}^{\theta_T} \sqrt{1 - \epsilon^2\cos^2\theta}\,\mathrm{d}\theta \tag{13}$$

where ϵ, θ, and a are defined, respectively, as

$$\epsilon = \frac{c}{a} \tag{14}$$

$$\theta_j = \tan^{-1}\left(\frac{\sqrt{a^2 - c^2}}{a}\tan\left(\tan^{-1}\left(\frac{y_j - y_0}{x_j - x_0}\right) - \lambda\right)\right), \quad j \in \{L, T\} \tag{15}$$

$$a = \frac{1}{2}\sqrt{((x_L - x_0) - c\cos\lambda)^2 + ((y_L - y_0) - c\sin\lambda)^2} + \ldots$$
$$\frac{1}{2}\sqrt{((x_L - x_0) + c\cos\lambda)^2 + ((y_L - y_0) + c\sin\lambda)^2} \tag{16}$$

As seen in Eqs. (14–16), the arc length of the ellipse is dependent on the same four variables that define the foci of the ellipse [Eq. (11)]. Once the arc length from Eq. (13) is known, the intercept time is simply

$$t_f = \frac{\mathbb{L}}{V} \tag{17}$$

Given the complexity of Eqs. (12) and (13), explicit solutions defining the ellipse that satisfies a specific γ_L^*, γ_T^*, and t_f^* have not been found. Therefore, a simplifying assumption is made that reduces the degrees of freedom from three to two and yields explicit solutions for elliptical trajectories that satisfy either γ_T^* and t_f^* or γ_T^* and γ_L^*. This special case is developed in the following subsection.

B. Special Case

An explicit representation of a subset of ellipses that satisfy a given γ_T^* and either t_f^* or γ_L^* is developed in this subsection. To draw an ellipse, four things are needed: the origin, the semi-major and semi-minor axes (a and b), and the rotation angle λ. This method starts by setting $\lambda = \gamma_T^*$. Next, the inertial Cartesian frame itself is rotated to match γ_T^*. An example of rotating the ellipse and the inertial Cartesian frame to match γ_T^* is displayed in Fig. 4.

Remark: All parameters in the rotated reference frame are denoted with prime notation.

Because the ellipse and the inertial Cartesian frame are rotated by the same angle λ, the ellipse can be represented as an unrotated ellipse in the rotated reference frame (see Fig. 4). This allows the parametric equations describing the ellipse in this rotated reference frame [Eq. (2)] to be simplified to

$$x' = -a\cos\theta + x_0' \tag{18a}$$

$$y' = b\sin\theta + y_0' \tag{18b}$$

The flight-path angle, relative to the rotated reference frame, can now be defined as

$$\tan\gamma' = \frac{\dot{y}'}{\dot{x}'} = \frac{b}{a\tan\theta} \tag{19}$$

where

$$\gamma' = \gamma - \lambda \tag{20}$$

Plugging Eq. (18) into Eq. (19) yields the general equation for the flight-path angle as a function of the missile's location on the ellipse:

$$\tan\gamma' = -\frac{b^2}{a^2}\frac{x' - x'_0}{y' - y'_0} \tag{21}$$

Rotating the ellipse to match γ_T^* places T at one of the vertices of the ellipse. This is important because, in the rotated frame $\gamma_T' = 0$, enabling closed-form equations to be developed. Equations (18) and (21) describe a subset of possible ellipses that satisfy γ_T^*. These equations are only a function of the y location of the ellipse's origin in the rotated frame (y_0') and are given as

$$x_0' = x_T' \tag{22}$$

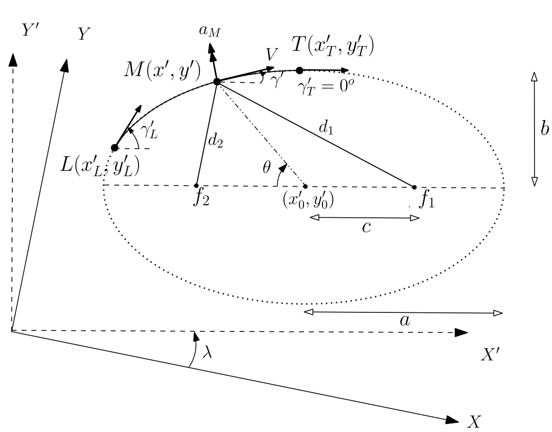

Fig. 4 Elliptical path geometry: rotated reference frame.

$$b = \sqrt{(y'_T - y'_0)^2} \tag{23}$$

$$a = \sqrt{\frac{(x'_L - x'_T)^2 (y'_T - y'_0)^2}{(y'_T - y'_0)^2 - (y'_L - y'_0)^2}} \tag{24}$$

$$\tan\gamma'_L = \frac{2y'_0(y'_T - y'_L) + y'^2_L - y'^2_T}{y'_0(x'_T - x'_L) + y'_L(x'_L - x'_T)} \tag{25}$$

The limits of y'_0 are found by evaluating the denominator of Eq. (24) and are dependent on the y values of T (y'_T) and L (y'_L) in the rotated reference frame. The value of θ for an unrotated ellipse is found by rearranging Eq. (18) and substituting in Eqs. (23) and (24) to give

$$\theta(x', y') = \tan^{-1}\left(\frac{-|(x'_L - x'_T)|}{\sqrt{(y'_T - y'_0)^2 - (y'_L - y'_0)^2}} \frac{(y' - y'_0)}{(x' - x'_T)}\right) \tag{26}$$

By plugging Eqs. (24) and (26) into Eq. (13), the length of the trajectory between the launcher and the target is shown to be only a function of y'_0. Therefore, by choosing a specific y'_0, the arc length [Eq. (13)] and intercept time [Eq. (17)] can be easily calculated. Once the desired ellipse is found in the rotated reference frame, the locations of the foci can be translated back into the inertial Cartesian frame using

$$x = x' \cos(-\lambda) + y \sin(-\lambda) \tag{27a}$$

$$y = -x' \sin(-\lambda) + y' \cos(-\lambda) \tag{27b}$$

It is important to emphasize that the ellipses generated from Eqs. (22–25) constitute only a subset of the possible solutions. This occurs for the special case because it is assumed that $\lambda = \gamma_T^*$, which reduces the degrees of freedom from three to two. Therefore, for a given γ_T, t_f is dependent on the value chosen for γ_L, and vice versa. The advantage of using the special case is that it yields closed-form solutions of the elliptical trajectories, albeit for a limited range of impact angles and intercept times. This method is still beneficial because the resultant elliptical trajectories can be used directly for the guidance law or as a valid initial guess to the numerical solver in the general case.

C. Trajectory Design Algorithm

The proposed solution strategy for finding the desired elliptical trajectory is portrayed in Algorithm 1. The process starts by defining γ_T^*. Equations (22–25) from the special case are used to find the elliptical trajectory that satisfies γ_T^* and t_f^*. If this resultant trajectory is satisfactory, either because $\gamma_L = \gamma_L^*$ or because the launcher has a variable launch angle, then the trajectory design process is complete.

If the resultant trajectory is not sufficient because $\gamma_L \neq \gamma_L^*$, then the special case trajectory that satisfies γ_L^* and γ_T^* is used instead. This new trajectory is used as the initial guess for solving the equations describing the general case [Eqs. (12) and (17)] to determine the elliptical trajectory that satisfies γ_L^*, γ_T^*, and t_f^*.

The successful implementation of Algorithm 1 assumes that the desired trajectory is achievable. It is important to note that not every combination of γ_L^*, γ_T^*, and t_f^* is possible. The values are dependent on each other as well as the relative distance and angle that L and T are from each other. Because of these five different variables (L, T, γ_L, γ_T, and t_f), the limit cases for all of the possible combinations are not shown.

That being said, there are two specific values of γ_T where unique solutions exist. When $\gamma_T^* = \xi$, the angle between T and L in the inertial Cartesian frame, the only possible solution connecting the two points is a straight line. Next, a singularity exists when $\gamma_T^* = \xi \pm \pi$, and there is no ellipse that connects L and T.

Algorithm 1 Determining foci for γ_T^*, γ_L^*, and t_f^*

1: **identify** locations of L and T
2: **choose** γ_T^*
3: **if** $\gamma_T^* \neq \xi + k\pi/2$, $k \in \mathbb{Z}$, **then**
4: **set** $\lambda = \gamma_T^*$
5: **choose** y'_0 corresponding to t_f^* [Eqs. (13), (24), and (26)]
6: **find** γ_L for given y'_0 (Eq. 25)
7: **if** $\gamma_L \neq \gamma_L^*$, **then**
8: **choose** y'_0 corresponding to γ_L^* [Eq. (25)]
9: **use** trajectory from step 8 as initial guess for numerical solver
10: **numerically solve** Eqs. (12) and (17) for λ, c, and (x_0, y_0) that satisfy t_f^*
11: **end if**
12: **return** Location of two foci f_1 and f_2 [Eq. (11)]
13: **end if**

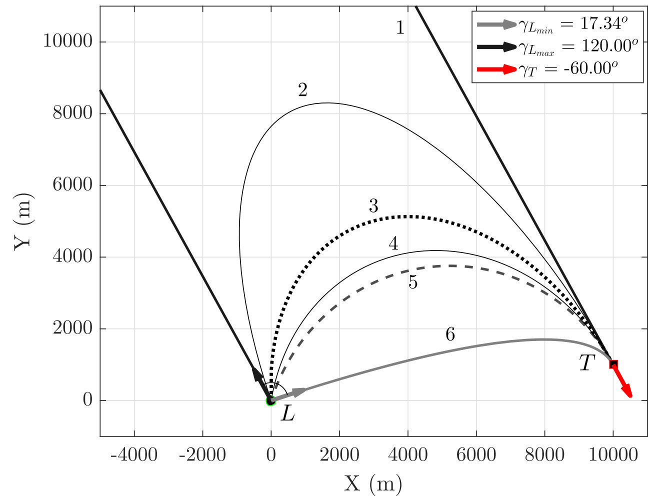

Fig. 5 Special case: range of elliptical trajectories for $\gamma_T^* = -60$ deg.

D. Case Study

In this subsection, a case study implementing Algorithm 1 is presented. A trajectory with $\gamma_L^* = 80$ deg, $\gamma_T^* = -60$ deg, and $t_f^* = 50$ s is desired. The launcher and the target are located at $L = [0, 0 \text{ m}]$ and $T = [10{,}000, 1000 \text{ m}]$, respectively, in the inertial Cartesian frame, and the interceptor's speed is assumed to be constant at $V = 300$ m/s.

The first step is to set $\lambda = \gamma_T^*$ and use the special case equations [Eqs. (22–25)] to find the value of y'_0 that corresponds to t_f^*. Figure 5 displays six different elliptical trajectories corresponding to different values of y'_0. The specific properties for each trajectory are shown in Table 1.

In Fig. 5, the lines 1 and 6 represent the limits of γ_L for the special case. When the two foci are collocated, the resulting trajectory is a circle (number 5) and is identical to the result of the inscribed angle method [30].

Specific to the case study, the dotted line (number 3) is the trajectory that achieves both $\gamma_T = -60$ deg and $t_f = 50$ s. However, the value of γ_L for the trajectory is 93.1 deg, which does not satisfy γ_L^* for the problem. The next step is to find the special case trajectory that satisfies γ_L^* and γ_T^* (number 4) and use it as the starting point for solving the general case equations [Eqs. (12) and (17)]. Successfully solving

Table 1 Trajectory properties for Fig. 5

Trajectory	t_f, s	γ_L, deg	y'_0, m
1	∞	120	$(y'_L + y'_T)/2 = 4580$
2	71.1	109.7	400
3	50	93.1	4110
4	44.4	80	3851
5	42.2	71.4	3647
6	34.7	17.34	$-\infty$

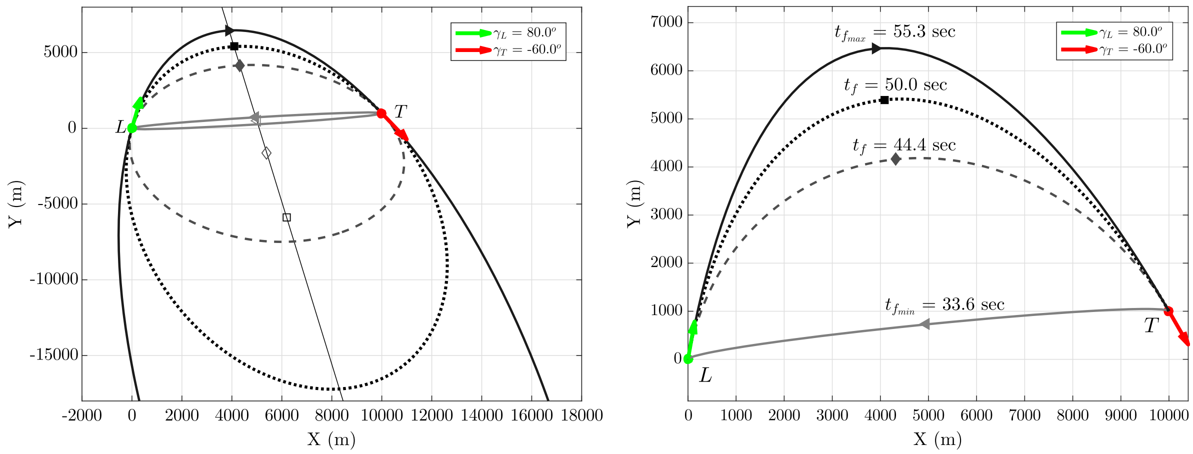

a) Range of Trajectories **b) Range of Trajectories (Zoomed In)**

Fig. 6 General case: range of elliptical trajectories for $\gamma_T^* = -60$ deg and $\gamma_L^* = 80$ deg.

Eqs. (12) and (17) yields the values of x_0, y_0, λ, and c and subsequently the foci of the desired ellipse [Eq. (11)]. A series of trajectories corresponding to $\gamma_L^* = 80$ deg and $\gamma_T^* = -60$ deg are plotted in Fig. 6 to illustrate the solution space for the numerical solver.

A unique property exists when finding the set of ellipses that intersect L and T at γ_L and γ_T. The angle between the origin and the midpoint of the trajectory $[(\theta_L + \theta_T)/2]$ is the same for every ellipse in the set. This is shown graphically in Fig. 6a, where a number of ellipses are plotted that achieve both γ_L^* and γ_T^*. For this particular case, the limits of λ are the angle between T and L ($\lambda_{\max} = \xi = 5.7$ deg) and the angle of the vertical line ($\lambda_{\min} = -79.4$ deg). Figure 6b is a zoomed-in version of Fig. 6a and plots the special case trajectory used as the initial guess for the numerical solver (dashed line) and the minimum and maximum intercept times, which correspond to the maximum and minimum values of λ (black and gray triangles, respectively). Most importantly, the solution trajectory that achieves $\gamma_L^* = 80$ deg, $\gamma_T^* = -60$ deg, and $t_f^* = 50$ s is plotted as the black dotted line in Fig. 6.

V. Guidance Law

The purpose of the guidance law is to maintain the interceptor along the desired elliptical trajectory by implementing the elliptical guidance concept. Functionally, the guidance concept is enforced by driving the error in Eq. (9) to zero. A linear guidance law is used because of the breadth of design and analysis tools available. The process of developing the linear control law is split into three sections. The first step is to define the nominal elliptical trajectory for a specific set of foci. Next, small deviations are assumed around this nominal trajectory, which allows the equations of motion to be linearized. Finally, a linear controller is developed that minimizes the missile's error from the nominal trajectory.

A. Nominal Elliptical Trajectory

A nominal ellipse is required to linearize the missile's nonlinear equations of motion and eventually design the controller. The ellipse is linearized in the polar frame (see Fig. 2), and the values of the states for the nominal trajectory are given as

$$d_1^* = \frac{\ell}{\rho} \tag{28}$$

where ℓ is called the semilatus rectum and is defined as

$$\ell = a(1 - \epsilon^2) \tag{29}$$

and ρ is

$$\rho = 1 + \epsilon \cos \psi^* \tag{30}$$

Remark: The asterisk denotes the parameters from the nominal trajectory corresponding to the ellipse that satisfies γ_L^*, γ_T^*, and t_f^*.

The rates of change of the two velocity components $V_{d_1}^*$ and V_ψ^* are given as

$$V_{d_1}^* = \dot{d}_1^* = \frac{\epsilon d_1^* \dot{\psi}^* \sin \psi^*}{\rho} \tag{31}$$

$$V_\psi^* = \dot{\psi}^* d_1^* \tag{32}$$

Because of the constant-speed assumption,

$$V = \sqrt{V_{d_1}^2 + V_\psi^2} \tag{33}$$

Plugging in Eqs. (31) and (32) into Eq. (33) yields

$$\dot{\psi}^* = -\frac{V\rho}{d_1^* \sqrt{1 + \epsilon^2 + 2\epsilon \cos \psi^*}} \tag{34}$$

Last, the nominal acceleration is defined in terms of the curvature

$$a_M^* = -V^2 \kappa \tag{35}$$

The curvature κ is defined in polar coordinates as

$$\kappa = \frac{|d_1^2 + 2d_\psi^2 - d_1 d_{\psi\psi}|}{(d_1^2 + d_\psi^2)^{3/2}} \tag{36}$$

where

$$d_\psi = \frac{\partial d_1^*}{\partial \psi^*} = \frac{\dot{d}_1^*}{\dot{\psi}^*}$$
$$d_{\psi\psi} = \frac{\partial^2 d_1^*}{\partial \psi^{*2}} = \frac{\epsilon d_1^*}{\rho^2}[\rho \cos \psi^* + 2\epsilon \sin^2 \psi^*] \tag{37}$$

Notice that the nominal trajectory defined in Eqs. (28–32) is only dependent on ψ^*. This means that, for any angle ψ, the corresponding values of d_1^*, $V_{d_1}^*$, V_ψ^*, and a_M^* can be easily found.

B. Linearization

The first step in the linearization process is determining the linear equations of motion relative to the nominal elliptical trajectory. The sum of the two distances D is the parameter used for the guidance law, but it is not included as one of the states. Therefore, the second step is to perform a transformation to change the existing states into the desired parameter D.

1. Equations of Motion

The linearized states of the system are

$$\Delta \boldsymbol{x} = [\,\Delta d_1 \quad \Delta V_{d_1} \quad \Delta V_\psi\,]^T \tag{38}$$

The equations of motion of these linearized states are defined as

$$\Delta \dot{\boldsymbol{x}} = \boldsymbol{A}(t)\Delta \boldsymbol{x} + \boldsymbol{B}(t)\Delta u \tag{39}$$

The values of $\boldsymbol{A}$ and $\boldsymbol{B}$ in Eq. (39) are found from taking the Jacobians of the equations of motion in Eqs. (3) and (4) for the states and controls, respectively, and are given as

$$\boldsymbol{A}(t) = \begin{bmatrix} 0 & 1 & 0 \\ \frac{-V_\psi^*(t)^2}{d_1^*(t)^2} & 0 & \left(\frac{2V_\psi^*(t)}{d_1^*(t)} - \frac{a_M^*(t)}{V}\right) \\ \frac{V_{d_1}^*(t)V_\psi^*(t)}{d_1^*(t)^2} & \left(-\frac{V_\psi^*(t)}{d_1^*(t)} + \frac{a_M^*(t)}{V}\right) & -\frac{V_{d_1}^*(t)}{d_1^*(t)} \end{bmatrix}$$

$$\boldsymbol{B}(t) = \begin{bmatrix} 0 \\ -\frac{V_\psi^*(t)}{V} \\ \frac{V_{d_1}^*(t)}{V} \end{bmatrix} \tag{40}$$

The linearized system in Eq. (39) is a linear time-varying (LTV) system that is a function of the time-dependent values of $d_1^*(t)$, $V_{d_1}^*(t)$, and $V_\psi^*(t)$.

2. Total Distance Transformation

The guidance concept is based on minimizing the deviation error in Eq. (9). In the linear formulation, this error is represented as ΔD. Because ΔD is not one of the states in Eq. (38), a transformation is performed to relate ΔD in terms of the known states. Assuming small deviations from the nominal ellipse allows

$$\Delta D(t) = \frac{\partial D^*}{\partial d_1^*}\Delta d_1(t) + \frac{\partial D^*}{\partial V_{d_1}^*}\Delta V_{d_1}(t) + \frac{\partial D^*}{\partial V_\psi^*}\Delta V_\psi(t) \tag{41}$$

where D^* is defined in Eq. (8), and its partial derivatives with respect to the different states are

$$\frac{\partial D^*}{\partial d_1^*} = 1 + \frac{d_1^* - 2c\cos\beta^*}{d_2^*} \tag{42a}$$

$$\frac{\partial D^*}{\partial V_{d_1}^*} = 0 \tag{42b}$$

$$\frac{\partial D^*}{\partial V_\psi^*} = 0 \tag{42c}$$

The time rate of change of the total distance error is found by taking the time derivative of Eq. (41)

$$\Delta \dot{D}(t) = \frac{d}{dt}\left(\frac{\partial D^*}{\partial d_1^*}\right)\Delta d_1(t) + \frac{\partial D^*}{\partial d_1^*}\Delta V_{d_1}(t) \tag{43}$$

where

$$\frac{d}{dt}\left(\frac{\partial D^*}{\partial d_1^*}\right) = \frac{d_2^*(\dot{d}_1^* + 2\dot{\beta}^* c\sin\beta^*) - \dot{d}_2^*(d_1^* - 2c\cos\beta^*)}{d_2^{*2}} \tag{44}$$

d_2 is defined in Eq. (5), and $\dot{\beta}$ and $\dot{d}_2^*$ are defined as

$$\dot{\beta} = -\frac{\psi\dot{\psi}}{|\psi|} \tag{45}$$

$$\dot{d}_2^* = \frac{\dot{d}_1^*(1 - 2c\cos\beta^*) + d_1^*(1 + 2c\dot{\beta}^*\sin\beta^*)}{d_2^*} \tag{46}$$

Using Eqs. (42a) and (44), the states Δd_1 and ΔV_{d_1} can be transformed into ΔD and $\Delta \dot{D}$:

$$\begin{bmatrix} \Delta D \\ \Delta \dot{D} \end{bmatrix} = \begin{bmatrix} \frac{\partial D^*}{\partial d_1^*} & 0 \\ \frac{d}{dt}\left(\frac{\partial D^*}{\partial d_1^*}\right) & \frac{\partial D^*}{\partial d_1^*} \end{bmatrix} \begin{bmatrix} \Delta d_1 \\ \Delta V_{d_1} \end{bmatrix} \tag{47}$$

Equation (47) effectively transforms the measured states of d_1 and V_{d_1} into the states required for the controller. Although V_ψ does not explicitly appear in this transformation, it still implicitly affects the values of ΔD and $\Delta \dot{D}$.

C. Guidance Law Design

The objective of the guidance law is to minimize ΔD. Figure 7 displays the guidance loop for the linearized system that drives ΔD to zero.

In the guidance loop, the controller receives ΔD and outputs a commanded acceleration a_M^c. This acceleration passes through an autopilot, and the nominal acceleration a_M^* is subtracted resulting in the acceleration difference Δu. This value of Δu is the input to the linearized equations of motion [Eq. (39)]. Although the system is linear, it is not time-invariant, which is problematic because it negates the use of stability analysis methods like root locus, Bode plots, and Nyquist criterion.

A proposed method for analyzing the stability of an LTV system is called the "frozen range" method [1]. In this method, the time-varying system is "frozen" for a specific time ($t = T_c$) and therefore can be evaluated as a linear time-invariant system. It should be noted that, although this method is convenient and intuitive, it does not always meet the sufficiency conditions for stability of the LTV system. Another approach (Gurfil et al. [36]) derives necessary and sufficient conditions for finite time stability of an LTV system. Both of these methods can be verified in simulation. For simplicity, and because the major thrust of this research is the guidance concept and not the specific guidance law, the frozen range method is used to demonstrate the viability of the proposed guidance law.

Using the frozen range method, the plant, evaluated at $t = T_c$, in transfer function form is

$$H(s) = \frac{\Delta D(s)}{\Delta u(s)} = \begin{bmatrix} \frac{\partial D^*}{\partial d_1^*}(T_c) & 0 & 0 \end{bmatrix}\begin{bmatrix} sI - \boldsymbol{A}(T_c) \end{bmatrix}^{-1}\boldsymbol{B}(T_c) \tag{48}$$

The output of the plant transfer function is ΔD, and a proportional–integral–derivative (PID) controller $G(s)$ is used to minimize ΔD in Fig. 7:

$$G(s) = K_P + \frac{K_I}{s} + sK_D \tag{49}$$

A PID controller is chosen as the guidance law because of its simplicity to implement and tune. The gains K_P, K_I, and K_D in Eq. (49) are for the proportional, integral, and derivative terms of the controller, respectively. To implement this guidance law, these gains need to be tuned to achieve the desired system response. The equivalent controller in the time domain is

$$a_M^c = K_P\Delta D + K_I\int \Delta D\,\mathrm{d}t + K_D\Delta \dot{D} \tag{50}$$

VI. Performance Analysis

Numerical simulations are used to evaluate the proposed elliptic guidance law. First, the linear model used for both the plant and the controller is validated against the nonlinear reference. Next, the validated linear PID controller is used to control a missile, with

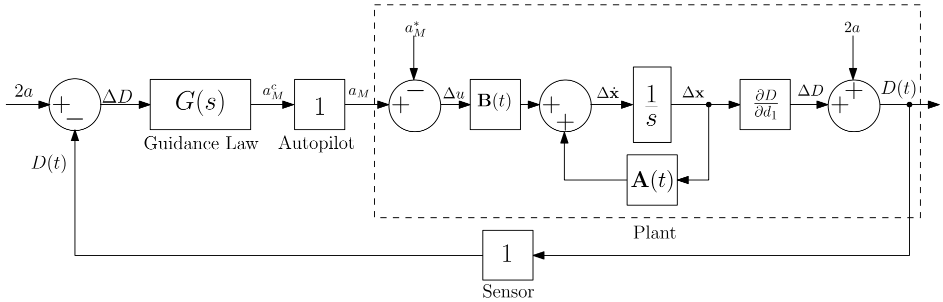

Fig. 7 Guidance loop diagram for elliptic guidance law.

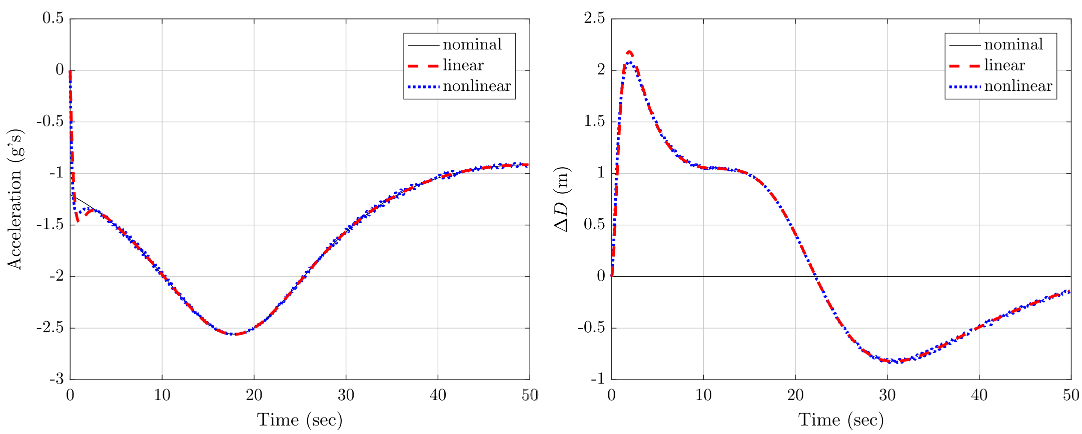

a) Acceleration Comparison (a_M)

b) Error Comparison (ΔD)

Fig. 8 Comparison of linear and nonlinear equations of motion.

nonlinear kinematics, to follow different elliptical trajectories. These trajectories correspond to specific values of t_f^* and γ_T^*. The chosen gains for the PID controller remain the same for both the validation process and the specific simulation scenarios. The specific gain values are $K_P = -5$, $K_I = -1$, and $K_D = -5$, and they are chosen using the root locus method to ensure closed-loop stability.

A. Linear Approximation Validation

In this subsection, the validity of the developed PID controller is tested. The same PID controller is simulated using the nonlinear equations of motion [Eqs. (3) and (4)] and using the linearized system in Eq. (39). Line number 3 from Fig. 5 is used as the nominal elliptical trajectory. The behaviors of both the linear and nonlinear systems are compared for a scenario with no heading error and ideal dynamics. In both simulations, the starting acceleration is zero. The results of the commanded acceleration verses time are plotted in Fig. 8a.

In Fig. 8, the dotted line represents the response of the nonlinear system, the dashed line corresponds to the response of the linear system, and the solid black line shows the acceleration [Eq. (35)] and distance error for the nominal trajectory. The important takeaway is that the accelerations and distance errors for both the linear and nonlinear equations are nearly identical. The close proximity of the simulated results for the linear and nonlinear equations of motion validates the linearization of the ellipse.

B. Nonlinear Simulations

Nonlinear simulations are performed using the linear PID guidance law. Three different missile scenarios (M_1, M_2, and M_3) are considered in the nonlinear simulation. Table 2 lists the desired objectives of each missile.

The objective of the simulation is to evaluate how γ_L^*, γ_T^*, and t_f^* impact the elliptical trajectories. The trajectory for M_1 serves as a baseline trajectory in that it shares a common t_f^* with M_2 and a common γ_T^* with M_3. The trajectories of all three missiles are plotted in Fig. 9a. For all the scenarios, the missile acceleration is limited to ± 10 g, and it uses a first-order autopilot with a time constant of $\tau = 0.1$ s. Additionally, a heading error of 20 deg is used to stress the controller.

The time-varying plots of each missile's actual and nominal accelerations are portrayed in Fig. 9b. In all three cases, the missile's acceleration initially saturates due to the presence of the 20 deg heading error but quickly stabilizes and remains within the g limits for the remainder of the engagement. The dip in acceleration around 44 s for M_1, 60 s for M_2, and 18 s for M_3 occurs when the missiles "turn the corner". This dip in acceleration has a negligible effect on the performance of the guidance law as long as the acceleration of the missile does not saturate during the turn. Despite the initial saturation, the PID controller is stable throughout the engagement and effectively implements the elliptic guidance concept for both desired intercept angles.

Figure 9c shows the time-varying values of each missile's γ. The initial spike in γ is seen as all three missiles maneuver from their respective γ_L and converge to their nominal trajectory. At the end of each missile's respective engagement ($t = t_f^*$), each missile intercepts the target at γ_T^*.

The values of ΔD are plotted with respect to time in Fig. 9d. The initial heading errors cause large deviation errors at the beginning of the engagement, but the guidance law is able to negate the deviation error after only two overshoots. Additionally, when M_1 and M_2 are "turning the corner", the accelerations are high enough that there is a small jump in ΔD. The PID controller is able to quickly minimize this error as well, allowing all three missiles to converge to the nominal trajectory and intercept the target with zero error.

Table 2 Initial conditions for the three nonlinear simulations

Simulation	γ_T^*, deg	γ_L^*, deg	t_f^*, s	Heading error, deg
M_1	−60	115.3	100	−20
M_2	−120	77	100	20
M_3	−60	93	50	−20

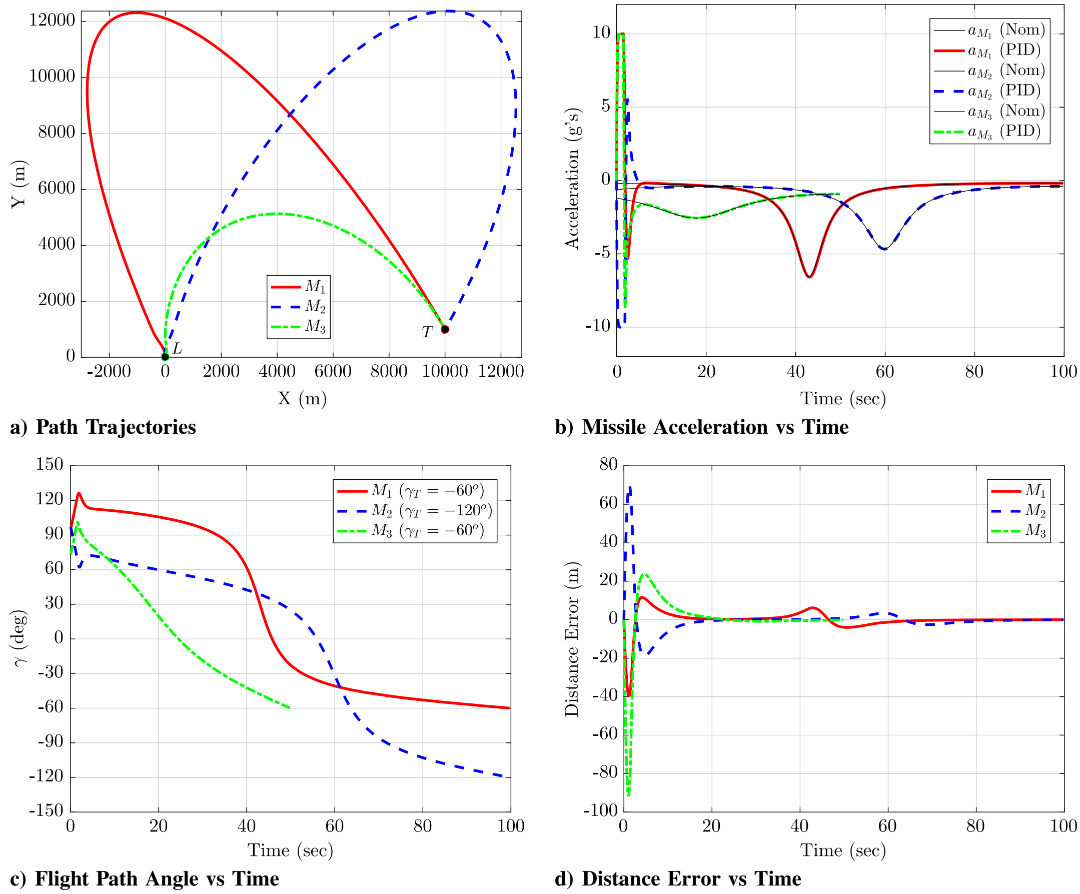

Fig. 9 Simulation results using PID controller ($K_P = -5$, $K_I = -1$, and $K_D = -5$).

VII. Conclusions

A new three-point, trajectory-shaping guidance concept against a stationary target was presented. This guidance concept was based on the elliptical geometric rule that the sum of the distances between any point on an ellipse and the two foci of that ellipse is constant. The equations for an ellipse that satisfied a desired launch angle, impact angle, and intercept time were presented. Closed-form equations were developed for a special case where the angle of rotation of the ellipse was set equal to the desired impact angle. These solutions constituted a subset of the possible elliptical trajectories and were valuable for trajectory planning or for using as an initial guess for the more general case. An algorithm was developed that outlined the process for finding an elliptical trajectory that satisfied a desired launch angle, impact angle, and intercept time. A case study demonstrated how the algorithm successfully converged to the desired elliptical trajectory.

A linear guidance law was chosen to implement the developed guidance concept. The equations of motion were linearized around a nominal elliptical trajectory, and a proportional–integral–derivative (PID) controller was used to drive the total distance error to zero. The stability of the PID controller was evaluated using the frozen range method, and the gains were chosen with root locus. The performance of this guidance law was evaluated with a nonlinear simulation of three different missile trajectories using first-order dynamics. The guidance law successfully overcame an initial 20 deg heading error and first-order dynamics to maneuver each interceptor to follow the desired elliptical trajectory. The success of the guidance law reinforced the viability of the linearization process, the frozen range method, and the PID gains for implementing the elliptic guidance concept. Furthermore, the successful performance of the guidance law in the different simulations showcased how the guidance concept could be used to enforce different impact angles for the same intercept time, and vice versa.

Acknowledgment

Riley Livermore and Ronny Tsalik were equally contributed to this paper.

References

[1] Shneydor, N. A., *Missile Guidance and Pursuit: Kinematics, Dynamics and Control*, Elsevier, Philadelphia, PA, 1998, pp. 47–75.

[2] Livermore, R., and Shima, T., "Deviated Pure Pursuit Based Optimal Guidance Law for Imposing Intercept Time and Angle," *Journal of Guidance, Control, and Dynamics* (to be published). doi:10.2514/1.G003179

[3] Ho, Y., Bryson, A., and Baron, S., "Differential Games and Optimal Pursuit-Evasion Strategies," *IEEE Transactions on Automatic Control*, Vol. 10, No. 4, 1965, pp. 385–389. doi:10.1109/TAC.1965.1098197

[4] Bryson, A., and Ho, Y., *Applied Optimal Control*, Blaisdell, Waltham, MA, 1969, Chap. 5.

[5] Zarchan, P., *Tactical and Strategic Missile Guidance*, 6th ed., AIAA, Reston, VA, 2007, pp. 13–34.

[6] Kim, M., and Grider, K. V., "Terminal Guidance for Impact Attitude Angle Constrained Flight Trajectories," *IEEE Transactions on Aerospace and Electronic Systems*, Vol. 9, No. 6, 1973, pp. 852–859. doi:10.1109/TAES.1973.309659

[7] Ryoo, C.-K., Cho, H., and Tahk, M.-J., "Optimal Guidance Laws with Terminal Impact Angle Constraint," *Journal of Guidance, Control, and Dynamics*, Vol. 28, No. 4, 2005, pp. 724–732. doi:10.2514/1.8392

[8] Shaferman, V., and Shima, T., "Linear Quadratic Guidance Laws for Imposing a Terminal Intercept Angle," *Journal of Guidance, Control, and Dynamics*, Vol. 31, No. 5, 2008, pp. 1400–1412. doi:10.2514/1.32836

[9] Cho, H., Ryoo, C.-K., Tsourdos, A., and White, B., "Optimal Impact Angle Control Guidance Law Based on Linearization About Collision Triangle," *Journal of Guidance, Control, and Dynamics*, Vol. 37, No. 3,

2014, pp. 958–964.
doi:10.2514/1.62910
[10] Jeon, I.-S., Lee, J.-I., and Tahk, M.-J., "Impact-Time-Control Guidance Law for Anti-Ship Missiles," *IEEE Transactions on Control Systems Technology*, Vol. 14, No. 2, 2006, pp. 260–266.
doi:10.1109/TCST.2005.863655
[11] Lee, J.-I., Jeon, I.-S., and Tahk, M.-J., "Guidance Law to Control Impact Time and Angle," *IEEE Transactions on Aerospace and Electronic Systems*, Vol. 43, No. 1, 2007, pp. 301–310.
doi:10.1109/TAES.2007.357135
[12] Kim, T.-H., Lee, C.-H., Jeon, I.-S., and Tahk, M.-J., "Augmented Polynomial Guidance with Impact Time and Angle Constraints," *IEEE Transactions on Aerospace and Electronic Systems*, Vol. 49, No. 4, 2013, pp. 2806–2817.
doi:10.1109/TAES.2013.6621856
[13] Kim, T.-H., Lee, C.-H., and Tahk, M.-J., "Time-to-Go Polynomial Guidance Laws with Terminal Impact Angle/Acceleration Constraints," *IFAC Proceedings Volumes*, Vol. 44, No. 1, 2011, pp. 3915–3919.
doi:10.3182/20110828-6-IT-1002.02304
[14] Lu, P., Doman, D. B., and Schierman, J. D., "Adaptive Terminal Guidance for Hypervelocity Impact in Specified Direction," *Journal of Guidance, Control, and Dynamics*, Vol. 29, No. 2, 2006, pp. 269–278.
doi:10.2514/1.14367
[15] Ratnoo, A., and Ghose, D., "Impact Angle Constrained Interception of Stationary Targets," *Journal of Guidance, Control, and Dynamics*, Vol. 31, No. 6, 2008, pp. 1817–1822.
doi:10.2514/1.37864
[16] Ratnoo, A., and Ghose, D., "Impact Angle Constrained Guidance Against Nonstationary Nonmaneuvering Targets," *Journal of Guidance, Control, and Dynamics*, Vol. 33, No. 1, 2010, pp. 269–275.
doi:10.2514/1.45026
[17] Ratnoo, A., "Analysis of Two-Stage Proportional Navigation with Heading Constraints," *Journal of Guidance, Control, and Dynamics*, Vol. 33, No. 1, 2015, pp. 269–275.
doi:10.2514/1.45026
[18] Kim, T.-H., Park, B.-G., and Tahk, M.-J., "Bias-Shaping Method for Biased Proportional Navigation with Terminal-Angle Constraint," *Journal of Guidance, Control, and Dynamics*, Vol. 36, No. 6, 2013, pp. 1810–1816.
doi:10.2514/1.59252
[19] Tekin, R., and Erer, K. S., "Switched-Gain Guidance for Impact Angle Control Under Physical Constraints," *Journal of Guidance, Control, and Dynamics*, Vol. 38, No. 2, 2014, pp. 205–216.
doi:10.2514/1.G000766
[20] Liu, X., Shen, Z., and Lu, P., "Closed-Loop Optimization of Guidance Gain for Constrained Impact," *Journal of Guidance, Control, and Dynamics*, Vol. 40, No. 2, 2017, pp. 453–460.
doi:10.2514/1.G000323
[21] Zhang, Y., Ma, G., and Liu, A., "Guidance Law with Impact Time and Impact Angle Constraints," *Chinese Journal of Aeronautics*, Vol. 26, No. 4, 2013, pp. 960–966.
doi:10.1016/j.cja.2013.04.037
[22] Shima, T., "Intercept-Angle Guidance," *Journal of Guidance, Control, and Dynamics*, Vol. 34, No. 2, 2011, pp. 484–492.
doi:10.2514/1.51026
[23] Utkin, V., "Variable Structure Systems with Sliding Modes," *IEEE Transactions on Automatic Control*, Vol. 22, No. 2, 1977, pp. 212–222.
doi:10.1109/TAC.1977.1101446
[24] Kumar, S. R., Rao, S., and Ghose, D., "Sliding-Mode Guidance and Control for All-Aspect Interceptors with Terminal Angle Constraints," *Journal of Guidance, Control, and Dynamics*, Vol. 35, No. 4, 2012, pp. 1230–1246.
doi:10.2514/1.55242
[25] Kumar, S. R., Rao, S., and Ghose, D., "Nonsingular Terminal Sliding Mode Guidance with Impact Angle Constraints," *Journal of Guidance, Control, and Dynamics*, Vol. 37, No. 4, 2014, pp. 1114–1130.
doi:10.2514/1.62737
[26] Harl, N., and Balakrishnan, S., "Impact Time and Angle Guidance with Sliding Mode Control," *IEEE Transactions on Control Systems Technology*, Vol. 20, No. 6, 2012, pp. 1436–1449.
doi:10.1109/TCST.2011.2169795
[27] Manchester, I. R., and Savkin, A. V., "Circular-Navigation-Guidance Law for Precision Missile/Target Engagements," *Journal of Guidance, Control, and Dynamics*, Vol. 29, No. 2, 2006, pp. 314–320.
doi:10.2514/1.13275
[28] Yoon, M.-G., "Relative Circular Navigation Guidance for Three-Dimensional Impact Angle Control Problem," *Journal of Aerospace Engineering*, Vol. 23, No. 4, 2010, pp. 300–308.
doi:10.1061/(ASCE)AS.1943-5525.0000043
[29] Yuan, L. C.-L., "Homing and Navigational Courses of Automatic Target-Seeking Devices," *Journal of Applied Physics*, Vol. 19, No. 12, 1948, pp. 1122–1128.
doi:10.1063/1.1715028
[30] Tsalik, R., and Shima, T., "Inscribed Angle Guidance," *Journal of Guidance, Control, and Dynamics*, Vol. 38, No. 1, 2014, pp. 30–40.
doi:10.2514/1.G000468
[31] Tsalik, R., and Shima, T., "Inscribed-Angle Guidance Against Moving Targets," *Journal of Guidance, Control, and Dynamics*, Vol. 40, No. 12, 2017, pp. 3211–3225.
doi:10.2514/1.G002786
[32] Siouris, G. M., *Missile Guidance and Control Systems*, Springer Science & Business Media, New York, 2004, Chap. 6.
[33] Zhang, T., and She, H., "Elliptical Trajectory Guidance Law with Terminal Impact Angle Constraint," *AIAA Atmospheric Flight Mechanics Conference*, AIAA Paper 2015-1021, 2015.
doi:10.2514/6.2015-1021
[34] Riedel, F. W., Hall, S. M., Barton, J. D., Christ, J. P., Funk, B. K., Milnes, T. D., Neperud, P. E., and Stark, D. R., "Guidance and Navigation in the Global Engagement Department," *Johns Hopkins APL Technical Digest*, Vol. 29, No. 2, 2010, pp. 118–132.
[35] Downs, J., *Practical Conic Sections: The Geometric Properties of Ellipses, Parabolas and Hyperbolas*, Courier Corp., Palo Alto, CA, 1993, Chap. 1.
[36] Gurfil, P., Jodorkovsky, M., and Guelman, M., "Finite Time Stability Approach to Proportional Navigation Systems Analysis," *Journal of Guidance, Control, and Dynamics*, Vol. 21, No. 6, 1998, pp. 853–861.
doi:10.2514/2.4348